

Prompt cusps and the dark matter annihilation signal

M. Sten Delos^{1*} and Simon D. M. White¹

^{1*}Max-Planck-Institut für Astrophysik, Karl-Schwarzschild-Str.
1, 85748 Garching, Germany.

*Corresponding author(s). E-mail(s): sten@mpa-garching.mpg.de;
Contributing authors: swhite@mpa-garching.mpg.de;

As gravitational collapse creates the first cosmic objects, a dark matter cusp forms immediately at every initial density maximum. Such prompt cusps have a density profile $\rho \propto r^{-1.5}$ extending up to a limiting density dependent on the nature of dark matter. Numerical simulations and theoretical arguments suggest that the bulk of these cusps survive until the present day. Here we show that if dark matter is a thermally produced weakly interacting massive particle, many thousands of prompt cusps with individual masses similar to that of the earth should be present in every solar mass of dark matter. This radically alters predictions for the amount and spatial distribution of dark matter annihilation radiation, substantially tightening observational constraints on the relevant cross sections. In particular, the cross section required to explain the Galactic Centre γ -ray excess predicts emission from prompt cusps elsewhere at levels in tension with the observed diffuse γ -ray background.

The most widely discussed class of dark matter models involve weakly interacting massive particles (WIMPs) that were thermally produced in the early universe and can therefore annihilate today in regions where the dark matter density is high [1, 2]. A variety of indirect detection experiments have now searched for annihilation products, typically γ -rays. As a two-body process, the annihilation rate within each volume element is proportional to the square of the local dark matter density, ρ . Consequently, most annihilation searches target the densest and nearest regions of space: our own Galactic Centre [3] and nearby dark matter-dominated satellite galaxies [4]. Intriguingly,

2 *Prompt cusps and dark matter annihilation*

an excess of γ -rays originating from the Galactic Centre has been identified [5] with an emission morphology that closely matches the prediction from high-resolution numerical simulations [6], although this signal has not been definitively attributed to dark matter.

The emission estimates underlying this search strategy neglect the contribution of unresolved dark matter substructure inside the target objects. Cold dark matter models predict the existence of gravitationally collapsed haloes down to earth mass or lower [7]. Since larger haloes assemble hierarchically from smaller ones, galaxy haloes contain many small subhaloes, the partially disrupted remnants of previous halo generations [8]. This substructure boosts their overall annihilation rate. Recent high-resolution numerical simulations [9] and semianalytic models [10] suggest that this effect is a factor of a few for objects like our Milky Way.

Recent results fundamentally change this picture, however. The first haloes form by the direct monolithic collapse of smooth peaks in the initial density field [11], a process that differs qualitatively from the gradual assembly that governs later halo growth [12]. The latter process yields halo density profiles with power-law indices that decrease monotonically towards halo centre, approaching $\rho \propto r^{-1}$ [13, 14] or even shallower [15, 16]. In contrast, prompt $\rho \propto r^{-1.5}$ density cusps form immediately at the moment of initial collapse of density peaks [17–22] and persist largely unaltered during subsequent halo growth, their inner boundary being set by the requirement that the local dark matter phase-space density cannot exceed its value at early times when the universe was almost uniform [22]. Since the annihilation rate inside a $\rho \propto r^{-1.5}$ cusp diverges logarithmically at small radii, the survival of these cusps has a major impact on the dark matter annihilation rate.

It is difficult to follow prompt cusps from their formation at $z \simeq 30$ until the present day. As time advances, most first generation haloes and their cusps are accreted onto larger objects, and the huge dynamic range in mass between the cusps and today’s galaxy-scale haloes makes fully self-consistent simulation of the process computationally intractable. Subhalo evolution has, however, been extensively studied using analytic methods and idealised simulations. While tidal forces gradually heat subhaloes and strip mass from their outer regions, theoretical descriptions of this process predict that even $\rho \propto r^{-1}$ density cusps survive unaltered at small radii [23–26]. Prompt cusps with $\rho \propto r^{-1.5}$ should be substantially more resistant to tidal effects [25, 27].

It is therefore expected that a large fraction of the initial prompt cusp population survives until the present day. Because they form so quickly after collapse of initial density peaks, prompt cusps have properties that are tightly linked to those of their peaks [20, 22]. A cusp’s mass is directly related to the comoving size of its peak, while its mean density is proportional to the mean density of the universe at the time the peak collapsed. Consequently, we can use the well-understood statistics of the population of initial density peaks [28] to quantify the statistics of the prompt cusp population. For a typical 100 GeV WIMP model, this calculation shows that tens of thousands of cusps should

form within each solar mass of dark matter. About 10 per cent of these cusps form by redshift $z = 32$, accounting for about 20 per cent of the final total mass in cusps, and for about 70 per cent of the final total annihilation luminosity. Figure 1 shows more broadly how the number, mass, and annihilation rate of cusps grow over time.

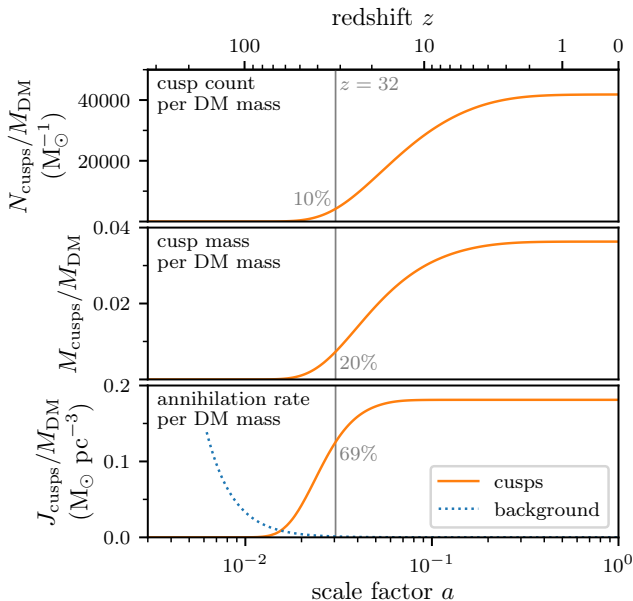


Fig. 1 The prompt cusp population as a function of time for a standard WIMP dark matter model. Normalized to the mass M_{DM} of dark matter (DM), the upper panel shows the cusp count N_{cusps} , the centre panel shows the total mass M_{cusps} in cusps, and the lower panel shows the total volume integrated squared density in cusps, J_{cusps} (Eq. 1), which is proportional to the total annihilation rate. By redshift $z = 32$ (gray vertical line), about 10 per cent of the prompt cusps have formed, but they contain 20 per cent of the final cusp mass and contribute 70 per cent of the final cusp annihilation luminosity. The annihilation rate is almost constant at $z < 20$. The lower panel also shows the annihilation rate predicted for homogeneous dark matter (dotted curve). The annihilation rate in cusps at late times is about 150 times the background rate at $z = 32$ and equal to that at $z = 175$.

The dark matter annihilation rate inside prompt cusps is proportional to the volume integral of the squared density,

$$J_{\text{cusps}} \equiv \int_{\text{cusps}} \rho^2 dV. \quad (1)$$

If we define z_{10} as the redshift by which 10 per cent of the cusps have collapsed, then we find that the annihilation J factor per unit dark matter mass M_{DM} , at $z = 0$, is

$$J_{\text{cusps}}/M_{\text{DM}} \simeq 150\bar{\rho}_0(1 + z_{10})^3, \quad (2)$$

4 *Prompt cusps and dark matter annihilation*

where $\bar{\rho}_0$ is the mean dark matter density today. This conclusion holds not only for the 100 GeV WIMP scenario considered in Fig. 1, for which we noted earlier that $z_{10} = 32$, but also for dark matter masses ranging from 1 GeV to 100 TeV, for which z_{10} ranges from 26 to 41. Thus prompt cusps dominate the annihilation rate from all present-day regions where they survive and where the dark matter density is less than a few million times the current cosmic mean.

The consequences of such a large annihilation rate are profound. Let us first evaluate the annihilation boost factor in dark matter haloes, which is the ratio of the annihilation rate arising from prompt cusps to the rate associated with the halo's smooth dark matter distribution. If $z_{10} = 32$, then Fig. 2 shows that the boost factor for haloes with Navarro-Frenk-White (NFW) density profiles [13, 14] ranges from 100 to 2500 as the NFW concentration parameter c is reduced from 20 (typical of dwarf galaxies) to 4 (typical of galaxy clusters). These factors are much larger than the order-unity values inferred for standard estimates of the properties of substructure in the absence of prompt cusps [9, 10].

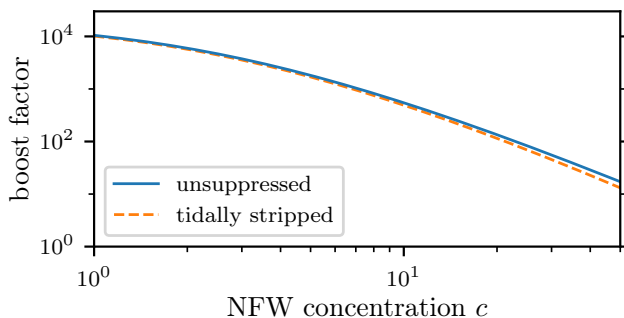


Fig. 2 Annihilation boost factor for NFW haloes due to prompt cusps at $z = 0$. We consider again a standard WIMP model with $z_{10} = 32$. The solid curve assumes that prompt cusps persist unaltered, while the dashed curve accounts for tidal stripping of the prompt cusps. The latter makes very little difference to the annihilation signal seen by a distant observer.

Another important consequence is that prompt cusps alter the predicted spatial distribution of the annihilation signal. When unresolved cusps dominate the signal, the annihilation rate in a volume element is proportional to the number of prompt cusps it contains and so to the first power of the mean dark matter density rather than to its square, as in the case of smoothly distributed dark matter. Fig. 3 shows the surface brightness from dark matter annihilation as a function of angular distance from the Galactic Centre, comparing the emission profile of the smooth halo to that of the prompt cusp population. We employ a recent Galactic halo mass model [29] and assume that all cusps survive, albeit modified by tides close to the Galactic Centre. Appropriately normalized, annihilation in this smooth halo closely matches the observed Galactic Centre γ -ray excess [30] (black points) out to nearly 20

degrees. Beyond the central 5 degrees, however, prompt cusps dominate the predicted signal and greatly enhance the emission at larger angles, already exceeding the observational upper limits at 20 degrees by almost an order of magnitude. Thus, unless the abundance and luminosity of prompt cusps are suppressed in the inner Galaxy by a much larger factor than we estimate, the observed emission profile of the Galactic Centre excess (GCE) is not consistent with that expected for annihilating dark matter.

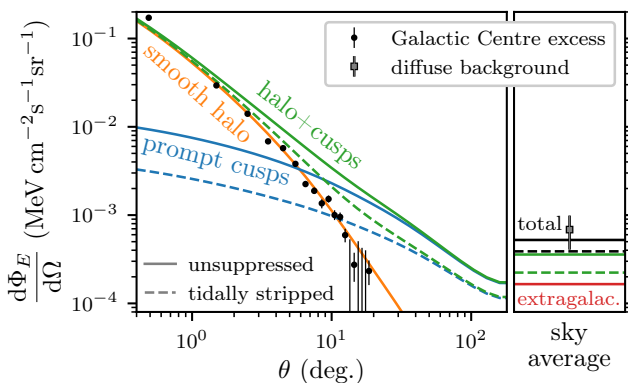


Fig. 3 Energy flux profile from dark matter annihilation in the Galactic halo. On the left, we compare the angular distribution that arises from the smooth halo (orange) to that arising from prompt cusps with $z_{10} = 32$ (blue). The measured Galactic Centre γ -ray excess in the 1 to 10 GeV range [30] (black points with 95 per cent confidence error bars) closely matches the smooth halo’s contribution out to nearly 20 degrees. However, annihilation in prompt cusps dominates over the smooth halo’s contribution outside the central few degrees, leading to a total flux profile (green) that exhibits a much shallower drop at large angles from the centre. Dashed curves show an estimate of the impact of tidal stripping on annihilation from prompt cusps, which is insufficient to modify this conclusion. On the right, we show the observed diffuse γ -ray background (point with error bar representing modeling uncertainty) integrated over the same energy range and averaged over Galactic latitudes $|b| > 20$ degrees [31]. Averaged over the same area of sky, the γ -ray flux arising from the Galactic halo (green) and from extragalactic dark matter (red) must account for a large fraction of the entire diffuse background in this energy range if the GCE is due to dark matter annihilation.

Since 20 degrees from the Galactic Centre corresponds to a distance of just 3 kpc, it is conceivable that prompt cusps suffer considerably more disruption in this region than we have estimated, particularly since encounters with individual stars are expected to remove the outer parts of many prompt cusps in star-dominated regions of the Galaxy. However, if the GCE were due to dark matter annihilation in the smooth halo, it would imply a cross section for producing observable γ rays which we can apply to prompt cusps in regions of lower density, where their survival prospects are clearer. In particular, the right-hand panel of Fig. 3 shows predictions for the mean energy flux from the Milky Way’s outer halo (at Galactic latitudes $|b| > 20$ degrees) and for the integrated emission from all extragalactic dark matter. These predictions can be compared to the observed diffuse γ -ray background [31] in the same 1

to 10 GeV energy range, which we show as a single point with an error bar to indicate its uncertainty. Clearly, if the GCE is due to dark matter annihilation, then the predicted backgrounds from prompt cusps in our galaxy and elsewhere must account for a large fraction of the entire diffuse 1 to 10 GeV background. Since most of this background is thought to be produced by discrete extragalactic sources such as star-forming galaxies and active galactic nuclei [32], an annihilation origin for the GCE is in serious tension with our current understanding of this background, and would predict it to have a significant large-scale variation across the sky.

Finally, we remark that the morphology of the annihilation signal from prompt cusps is essentially the same as that of a signal from dark matter decay, so one can straightforwardly convert any lower bound on the dark matter lifetime τ into an upper limit on the annihilation cross section $\langle\sigma v\rangle$. As an illustration, we consider a set of lower bounds on τ that employ the diffuse γ -ray background [32]. For the particular example of annihilation into $b\bar{b}$, the resulting upper bounds on $\langle\sigma v\rangle$ are shown in Fig. 4 as a function of the dark matter particle mass m_χ . We also plot the thermal relic cross section $\langle\sigma v\rangle$ (horizontal dotted line) that is required to yield the observed dark matter abundance [33] (assuming a standard thermal history [34]). These bounds evidently rule out thermal relics up to masses of more than 10 TeV, far more stringent than previous limits that do not account for the prompt cusps [3, 4].

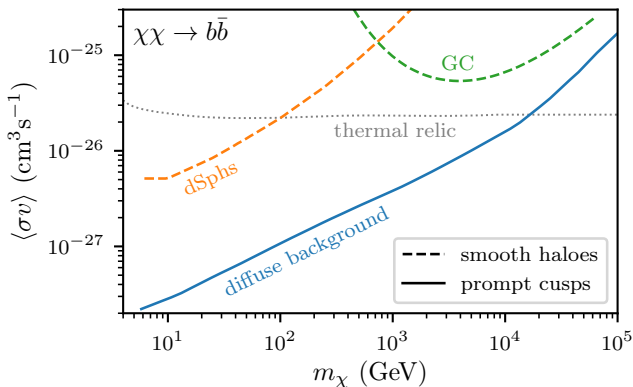


Fig. 4 Comparing bounds on dark matter annihilation in prompt cusps to previous bounds that consider smooth haloes. We specialize to the $b\bar{b}$ annihilation channel and plot the annihilation cross section $\langle\sigma v\rangle$ against the particle mass m_χ . The solid curve shows the upper limit on $\langle\sigma v\rangle$ due to annihilation in Galactic and extragalactic prompt cusps based on the Fermi collaboration’s measurement of the diffuse γ -ray background [31] after subtraction of other astrophysical contributions [32]. The dashed curves show the upper bounds that arise from limits on annihilation inside the smooth haloes of dwarf spheroidal galaxies (dSphs) [4] and the Galactic Centre (GC) [3]. We show 95 per cent confidence limits in all cases. Evidently, prompt cusps enable bounds on dark matter annihilation that are stronger than previous limits by more than an order of magnitude. The dotted curve shows the cross section that yields the observed dark matter abundance for thermal relic WIMPs [33]; candidates less massive than 10 TeV are excluded.

Methods

Power spectrum. To evaluate the prompt cusp distribution, the first step is to fix the power spectrum $P(k)$ of linear density fluctuations. Adopting the cosmological parameters measured by the Planck mission [35], we compute the power spectrum of cold dark matter at $z = 31$ using the CLASS Boltzmann solver [36] and extrapolate it to unresolved small scales using the exact small-scale growth function valid in mixed matter-radiation domination [37]. Next, we fix the mass m_χ of the dark matter particle and the temperature T_{kd} at which it kinetically decouples from the Standard Model radiation bath. We then evaluate the free-streaming length k_{fs}^{-1} and scale the power spectrum by $\exp(-k^2/k_{\text{fs}}^2)$ [38].

Figure 5 shows the power spectrum at $z = 31$ for the scenario with $m_\chi = 100$ GeV and $T_{\text{kd}} = 30$ MeV, which is the standard WIMP model that we adopt in the main text. The free-streaming wavenumber in this case is $k_{\text{fs}} = 1.06 \times 10^6$ Mpc⁻¹. The feature at $k \simeq 10^3$ Mpc⁻¹ marks the baryon clustering limit. At larger scales $k \lesssim 10^{-3}$ Mpc⁻¹, baryons cluster with the dark matter, and perturbations grow at the usual rate $\delta \propto a$, where a is the cosmic expansion factor. At smaller scales $k \gtrsim 10^{-3}$ Mpc⁻¹, baryons are a smooth background, and perturbations grow at the rate $\delta \propto a^g$ with $g \simeq 0.901$ [37]. In the analysis below, we approximate that $\delta \propto a^{0.901}$ at all the (small) scales of interest.

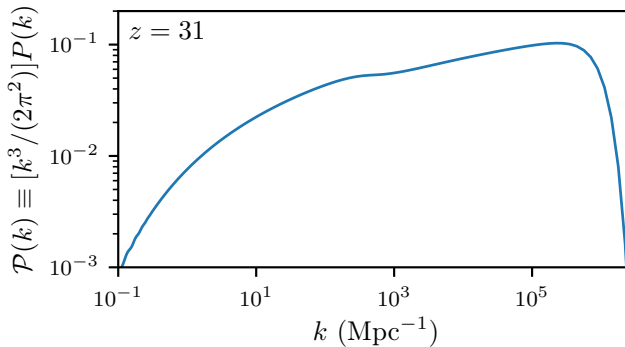


Fig. 5 Dimensionless power spectrum $\mathcal{P}(k)$ of dark matter density variations in a standard WIMP scenario at $z = 31$. Specifically we take $m_\chi = 100$ GeV and $T_{\text{kd}} = 30$ MeV, which leads to $k_{\text{fs}} = 1.06 \times 10^6$ Mpc⁻¹.

Peak and cusp distribution. Given an initial peak in the density contrast field $\delta \equiv \delta\rho/\bar{\rho}$, the prompt cusp it forms has the density profile $\rho = Ar^{-1.5}$ with [22]

$$A \simeq 24\bar{\rho}_0 a_{\text{coll}}^{-1.5} R^{1.5}. \quad (3)$$

Here, $\bar{\rho}_0$ is the mean dark matter density today, a_{coll} is the expansion factor at the peak's collapse, and $R \equiv |\delta/\nabla^2\delta|^{1/2}$ is the peak's characteristic comoving size. In particular, if $\delta(a)$ is the peak height at some scale factor a , then the collapse scale factor is $a_{\text{coll}} = [f_{\text{ec}}(e, p)\delta_c/\delta(a)]^{1/g} a$, where $\delta_c = 1.686$ is the

8 *Prompt cusps and dark matter annihilation*

critical density contrast for collapse of a spherical perturbation, $g \simeq 0.901$ is the growth index at small scales, and $f_{ec}(e, p)$ is the ellipsoidal collapse correction, approximated as [39]

$$f_{ec}(e, p) = 1 + 0.47 [5(e^2 - p|p|)f_{ec}^2(e, p)]^{0.615}, \quad (4)$$

which depends on the ellipticity e and prolateness p of the tidal field at the peak. Note that f_{ec} grows to more than 5 as $e^2 - p|p|$ approaches 0.26, and Eq. (4) has no solution when $e^2 - p|p| > 0.26$. We therefore neglect any peaks for which $e^2 - p|p| > 0.26$.¹

With the power spectrum fixed, we can straightforwardly employ the statistics of peaks to quantify how δ , $\nabla^2\delta$, e and p are distributed [20]. For convenience, we reproduce the relevant equations, which are expressed in terms of $\sigma_j^2 \equiv \int \frac{dk}{k} \mathcal{P}(k) k^{2j}$, $R_* \equiv \sqrt{3}\sigma_1/\sigma_2$, and $\gamma \equiv \sigma_1^2/(\sigma_0\sigma_2)$. Here $\mathcal{P}(k) \equiv [k^3/(2\pi^2)]P(k)$ is the dimensionless dark matter power spectrum (e.g. Fig. 5). The differential number density of peaks, in terms of parameters $\nu \equiv \delta/\sigma_0 > 0$ and $x \equiv -\nabla^2\delta/\sigma_2 > 0$, is [28]

$$\frac{d^2 n_{\text{peaks}}}{d\nu dx} = \frac{e^{-\nu^2/2}}{(2\pi)^2 R_*^3} f(x) \frac{\exp[-\frac{1}{2}(x - \gamma\nu)^2/(1 - \gamma^2)]}{[2\pi(1 - \gamma^2)]^{1/2}}, \quad (5)$$

$$f(x) \equiv \frac{x^3 - 3x}{2} \left[\text{erf}\left(\sqrt{\frac{5}{2}}x\right) + \text{erf}\left(\sqrt{\frac{5}{8}}x\right) \right] + \sqrt{\frac{2}{5\pi}} \left[\left(\frac{31}{4}x^2 + \frac{8}{5}\right) e^{-\frac{5}{8}x^2} + \left(\frac{x^2}{2} - \frac{8}{5}\right) e^{-\frac{5}{2}x^2} \right]. \quad (6)$$

Given peak height ν , the distribution of e and p can be taken to be² [39]

$$f(e, p | \nu) = \frac{1125}{\sqrt{10\pi}} e(e^2 - p^2)\nu^5 \exp\left[-\frac{5}{2}\nu^2(3e^2 + p^2)\right]. \quad (7)$$

For each WIMP scenario that we study, we generate a sample of 10^7 peaks, using rejection methods to sample δ and $\nabla^2\delta$ and inverse transforms to sample e and p . We also integrate Eq. (5) to find the number density n_{peaks} of peaks. Figure 6 shows the resulting distribution of peaks (left-hand panel) for the WIMP scenario considered in Fig. 5. Now for each peak, we use Eq. (3) to

¹In the scenario with $m_\chi = 100$ GeV and $T_{\text{kd}} = 30$ MeV, 53 per cent of the peaks have $e^2 - p|p| > 0.26$ and are therefore ignored. These peaks are still expected to collapse; it is only the approximation in Eq. (4) that breaks down. Neglecting these peaks does not significantly affect our results, however. Peaks with $e^2 - p|p| > 0.26$ are on average about a third as high as the other peaks, so even if they were spherical, they would collapse much later and so form much less dense cusps. In particular, the annihilation rate in a peak's prompt cusp is proportional to $\delta^{3.3}R^3$ if ellipsoidal collapse is neglected. The sum of $\delta^{3.3}R^3$ over peaks with $e^2 - p|p| > 0.26$ is under three per cent of the total. Note that the numbers in Fig. 1 refer to the peaks which *do* collapse according to Eq. (4).

²Equation (7) describes the distribution of e and p at an arbitrary point; the distribution restricted to density peaks is not known.

evaluate the density coefficient A , and we also evaluate

$$r_{\text{cusp}} = 0.11 a_{\text{coll}} R, \quad (8)$$

which is roughly the outer radius of the prompt cusp, at least to within a factor of a few [22]. The annihilation rate is only logarithmically sensitive to this parameter. The right-hand panel of Fig. 6 shows the distribution of cusps in mass M_{cusp} and radius r_{cusp} , where $M_{\text{cusp}} = (8\pi/3)Ar_{\text{cusp}}^{1.5}$ is the mass enclosed within r_{cusp} .

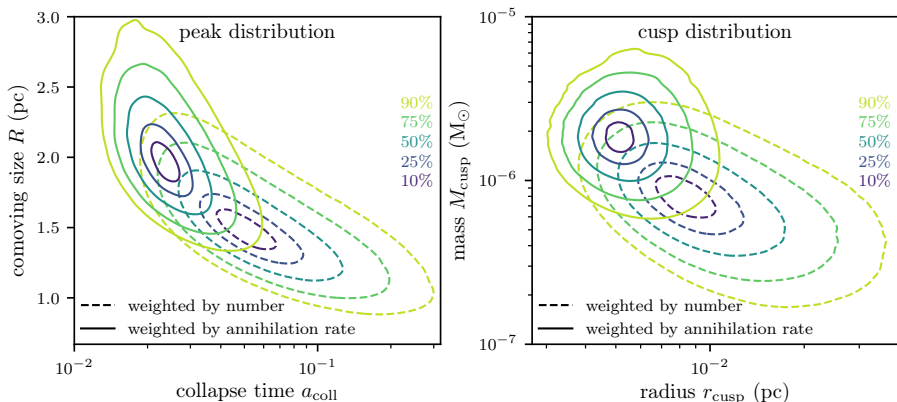


Fig. 6 Distribution of peaks (left-hand panel) and the resulting prompt cusps (right-hand panel) in the standard WIMP scenario with $m_\chi = 100$ GeV and $T_{\text{kd}} = 30$ MeV. We show contours that enclose 10, 25, 50, 75, and 90 per cent of the distribution. Dashed contours are weighted by the number of cusps, while solid contours are weighted by the annihilation rate. The cusp sizes R tend to lie within a factor of a few of the free-streaming scale $k_{\text{fs}}^{-1} = 0.94$ pc. Prompt cusps arising from earlier-forming and larger initial peaks tend to dominate the annihilation rate; they end up at the high end of the cusp mass distribution and the low end of the radius distribution. Only peaks with $e^2 - p|p| > 0.26$ are considered here (see footnote 1).

We consider a number of WIMP scenarios with different m_χ and T_{kd} . Figure 7 shows the redshift z_{10} by which 10 per cent of the cusps have collapsed.³ This number largely determines the annihilation rate in cusps; see Eq. (2). Generally, larger particle masses and earlier decoupling cause cusps to form earlier because both effects move the free-streaming cutoff k_{fs}^{-1} to smaller scales, where there is (logarithmically) more power in density variations.

The final feature of each prompt cusp is the interior radius at which the $\rho = Ar^{-1.5}$ cusp gives way to a central core [22]. This feature is enforced by Liouville's theorem, which implies that the maximum phase-space density f_{max} set in the early universe cannot be exceeded inside collapsed structures. For

³We take z_{10} to be the redshift by which 10 per cent of the peaks with $e^2 - p|p| < 0.26$ have collapsed, since we are able to associate these peaks with prompt cusps; see footnote 1. z_{10} corresponds to roughly the redshift by which 5 per cent of all peaks have collapsed.

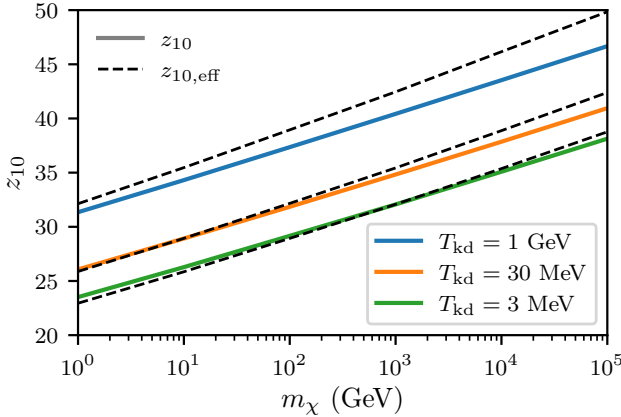


Fig. 7 Redshift z_{10} (solid curves) by which 10 per cent of the cusps have collapsed, for various WIMP dark matter models. We also show the effective value $z_{10,\text{eff}}$ that makes Eq. (2) correct (dashed curves).

dark matter that decoupled while it was nonrelativistic at the scale factor a_{kd} ,

$$f_{\text{max}} = (2\pi)^{-3/2} (m_\chi/T_{\text{kd}})^{3/2} \bar{\rho}_0 a_{\text{kd}}^{-3}, \quad (9)$$

and the phase-space structure of a $\rho = Ar^{-1.5}$ cusp implies that f_{max} is reached at the radius r_{core} where

$$Ar_{\text{core}}^{4.5} \simeq 3 \times 10^{-5} G^{-3} f_{\text{max}}^{-2}. \quad (10)$$

For WIMP dark matter scenarios, $r_{\text{cusp}}/r_{\text{core}} \sim 500$ for most prompt cusps, which implies that the $\rho \propto r^{-1.5}$ density profile extends over about that factor in radius. Below r_{core} , we assume that prompt cusps possess uniform density $\rho = Ar_{\text{core}}^{-1.5}$.

Annihilation in prompt cusps. The annihilation J factor (Eq. 1) inside a given prompt cusp is

$$J = (4\pi/3)A^2 [1 + 3 \log(r_{\text{cusp}}/r_{\text{core}})]. \quad (11)$$

The number of cusps per dark matter mass is the ratio $n_{\text{cusps}}/\bar{\rho}$ between the cusp number density and the mean dark matter density. Note that $n_{\text{cusps}} = f_{\text{coll}}n_{\text{peaks}}$, where f_{coll} is the fraction of peaks that have collapsed by the time under consideration (and recall that some peaks are taken never to collapse, owing to Eq. 4 having no solution for them). The annihilation J factor per mass is then $J_{\text{cusps}}/M_{\text{DM}} = \bar{J}n_{\text{cusps}}/\bar{\rho}$, where \bar{J} is the average value of Eq. (11) over the cusps that have collapsed. We have added to Figure 7 the effective value $z_{10,\text{eff}}$ (dashed curves) that makes Eq. (2) yield the correct annihilation rate per dark matter mass. Generally, $z_{10,\text{eff}}$ grows slightly more quickly than z_{10}

because as the free-streaming cutoff k_{fs}^{-1} moves to smaller scales, the (dimensionless) power spectrum near the cutoff becomes shallower, which makes peak sizes R slightly larger in relation to k_{fs}^{-1} .

We can evaluate the same annihilation J factor for a much more massive halo with an NFW density profile

$$\rho(r) = \frac{\rho_s}{r/r_s(1+r/r_s)^2}. \quad (12)$$

The annihilation boost factor due to prompt cusps inside that halo, assuming full cusp survival, is just $(J_{\text{cusps}}/M_{\text{DM}})/(J_{\text{halo}}/M_{\text{halo}})$. Figure 2 shows this boost factor at $z = 0$ for haloes with NFW concentration parameter $c = R_{200}/r_s$, where R_{200} is the radius that encloses average dark matter density 200 times the cosmological mean, together with boost factor obtained if prompt cusps close to halo centre are assumed to be tidally truncated as described below. The cusps are so compact compared to late-time massive haloes that tidal truncation has very little effect on the overall boost factors.

Galactic halo. To explore annihilation signals from the Galactic halo, we use a recent mass model [29] that is tuned to match observational data. At poorly constrained small scales, this model employs a simulation-tuned prescription to describe how the dark matter halo contracts due to domination by baryons in the central region. The Sun is taken to reside at $r_0 = 8.20$ kpc. Figure 8 shows the density profile associated with this model. Note that the prescription for halo contraction has not been validated at radii below 1 kpc, so the density profile in that regime represents an extrapolation.

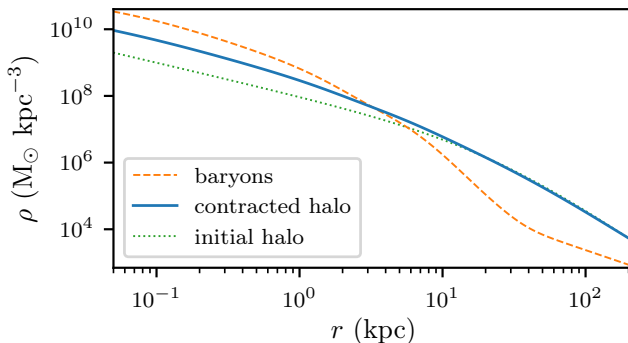


Fig. 8 Spherically averaged Galactic density profile associated with the observationally tuned mass model that we use [29]. Dominance of baryons (dashed curve) at small radii causes the dark matter’s initial NFW density profile (dotted curve) to contract (solid curve).

Tidal stripping of prompt cusps. Near the centre of the Galactic halo and other dark matter haloes, prompt cusps can be gradually stripped by tidal forces, an effect that reduces their annihilation signal. Previous numerical

studies have explored the impact of tidal evolution on subhalo annihilation rates [40, 41], but they assumed NFW density profiles, so their results cannot be directly applied to prompt cusps. For example, a prompt cusp’s annihilation rate is only logarithmically sensitive to its outer radius, and so is only weakly affected by loss of outer material. Also, steeper cusps are more resistant to tidal effects than those of NFW haloes [27].

However, several theoretical models of tidal evolution have been developed [23–26]. All of these models predict that a central cusp should remain intact at sufficiently small radii, even as a subhalo’s outer regions expand and are stripped. We use the ADIABATIC-TIDES model [25] to explicitly evaluate the suppression of a prompt cusp’s annihilation rate due to tidal stripping. This model describes the density profile of the asymptotic tidal remnant of a subhalo with a set initial profile. Specifically, we evaluate the tidal remnant of an idealized $\rho \propto r^{-3/2}$ power law density profile (which has no truncation or core radius). Since the idealized profile is scale-free, the result can be straightforwardly rescaled to apply to any prompt cusp in any region of any halo. To appropriately account for the core radius r_{core} and the cusp’s outer radius r_{cusp} , we next scale the tidally stripped idealized profile by the ratio between the cusp’s initial profile and the initial idealized power law. That is, below r_{core} we scale the tidally stripped density profile by $(r/r_{\text{core}})^{3/2}$, and we truncate the profile at the outer radius r_{cusp} . This procedure is not exact, but we have verified that alternative procedures (like truncating at the cusp mass M_{cusp} instead of the cusp radius) do not change the resulting annihilation rate significantly.

The degree of stripping in the ADIABATIC-TIDES model depends on the subhalo’s pericentre radius. For our standard WIMP scenario, Fig. 9 shows the factor by which tidal stripping by the total Galactic potential (including baryons), shown in Fig. 8, suppresses annihilation inside prompt cusps as a function of their pericentre radii. We comment that for this Galactic mass distribution, the ADIABATIC-TIDES model predicts that the impact of tidal stripping begins to weaken as the pericentre radius drops below 0.24 kpc. This effect arises because the shallowing of the density profile at these radii causes the radial tidal force to weaken. While this effect may be real, we conservatively neglect it and assume that prompt cusps with pericentres below 0.24 kpc are tidally stripped to the same degree as those with pericentres at 0.24 kpc. Note that at the distance to the Galactic Centre, 0.24 kpc corresponds to 1.7 degrees on the sky.

Within an isothermal sphere, which has the density profile $\rho \propto r^{-2}$ and is typically a good approximation for a large range of radii inside Galactic systems, the average pericentre radius of particles at radius r is about $r_{\text{peri}} \simeq 0.55r$. The average value of r_{peri}/r is higher for the shallower profiles relevant to haloes’ deep interiors. We approximate a prompt cusp’s pericentre radius as half of its current radius, so we scale the annihilation rate in prompt cusps at the radius r by the tidal scaling factor (e.g. in Fig. 9) evaluated for the pericentre $r/2$. With this scaling applied, the factors by which the sky-averaged

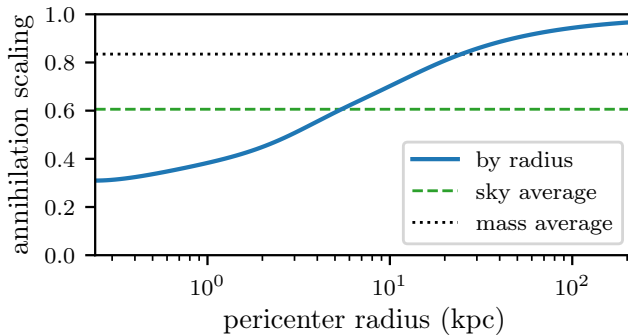


Fig. 9 Impact of tidal stripping on the annihilation rate in prompt cusps in the Galactic halo. As a function of the Galactic pericentre radius, the solid curve shows the factor by which the annihilation rate, summed over the full prompt cusp distribution, is scaled, according to the ADIABATIC-TIDES model [25]. We consider the WIMP scenario with $m_\chi = 100$ GeV and $T_{\text{tid}} = 30$ MeV. The dashed curve shows the factor by which the sky-averaged prompt cusp annihilation rate is suppressed, where we specifically average over angles for which the Galactic latitude $|b| > 20$ degrees (as in Fig. 3). The dotted curve shows the factor by which the total annihilation rate of prompt cusps in the Galactic halo is suppressed. For the latter lines, we assume that a prompt cusp’s pericentre radius is half of its current radius.

and mass-averaged annihilation rates are suppressed in prompt cusps in the Galactic halo are also shown in Fig. 9. We show the tidally scaled prompt cusp signal from the Galactic halo in Fig. 3.

We also repeat this calculation for arbitrary NFW host haloes. The dashed curve in Fig. 2 shows annihilation boost factors if tidal stripping is taken into account. Clearly, its overall impact is minimal.

γ -ray spectra. The energy spectrum of the Galactic Centre γ -ray excess between 1 and 10 GeV is well fit by a log-parabola [30]. In order to attribute the Galactic Centre excess to dark matter annihilation in the smooth Galactic halo, as shown in Fig. 3, the differential photon power emitted by a mass M_{DM} of dark matter with density ρ must be

$$E^2 \frac{dN}{dE} = \mathcal{N}_{\text{GCE}}(E) \frac{M_{\text{DM}}}{M_\odot} \frac{\rho}{M_\odot \text{Mpc}^{-3}}, \quad (13)$$

where

$$\mathcal{N}_{\text{GCE}}(E) = 8.6 \times 10^{14} \text{ MeV s}^{-1} \left(\frac{E}{\text{GeV}} \right)^{0.27 - 0.27 \log\left(\frac{E}{\text{GeV}}\right)} \quad (14)$$

is a rescaled form of the same log-parabola. For prompt cusps, we replace ρ with the effective density $J_{\text{cusps}}/M_{\text{DM}}$.

For a line-of-sight angle Ω , the energy flux from the Galactic halo is

$$E \frac{d^2\Phi_E}{d\Omega dE} = \frac{1}{4\pi} \mathcal{N}_{\text{GCE}}(E) \int_0^\infty dl \left[\frac{J_{\text{cusps}}}{M_{\text{DM}}} \rho(l, \Omega) + \rho(l, \Omega)^2 \right], \quad (15)$$

where $\rho(\ell, \Omega)$ is the density of the smooth halo. The sum accounts for both the smooth halo and the prompt cusps. To evaluate the Galactic contribution to the diffuse γ -ray background, we average Eq. (15) over the portion of the sky for which the Galactic latitude $|b| > 20$ degrees. The extragalactic contribution to this background is

$$E \frac{d^2\Phi_E}{d\Omega dE} = E^2 \frac{c}{4\pi} \bar{\rho}_0 \frac{J_{\text{cusps}}}{M_{\text{DM}}} \int_0^\infty \frac{dz}{H(z)} \left[\frac{\mathcal{N}_{\text{GCE}}(E')}{E'^2} \right]_{E'=E(1+z)}, \quad (16)$$

where we neglect scattering with extragalactic background light, which is minor at these energies.⁴ The resulting differential energy spectra are plotted in Fig. 10 along with that of the measured diffuse γ -ray background [31], and the right-hand panel of Fig. 3 shows these components integrated over the the 1 to 10 GeV energy range. As we noted in the main text, dark matter in this scenario is required to account for a large fraction of the diffuse γ -ray flux in this range, which is incompatible with prior results indicating that nearly all of the diffuse flux can be attributed to astrophysical sources [32].

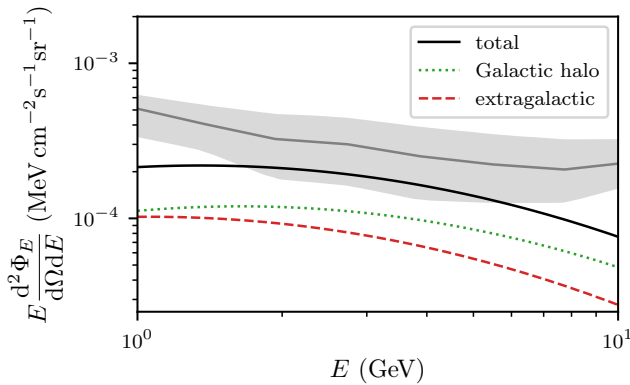


Fig. 10 Contribution of dark matter annihilation to the diffuse γ -ray background if the Galactic Centre γ -ray excess is attributed to annihilation in the smooth Galactic halo. We consider a WIMP scenario with $z_{10} = 32$. We show the measured diffuse flux (gray curve with modeling uncertainty band) along with the predicted contribution of the Galactic halo (dotted curve; including the effect of tidal stripping), that of extragalactic dark matter (dashed curve), and the sum of the two contributions (black solid curve).

Conversion of limits on the dark matter lifetime. Given a lower limit on the lifetime τ of a dark matter candidate with mass $m'_\chi = 2m_\chi$, we can derive an upper limit on the annihilation cross section $\langle\sigma v\rangle$ of a (different) dark matter candidate with mass m_χ by equating the annihilation and decay

⁴We also evaluated the extragalactic contribution using the γ -CASCADE code [42], which accounts for scattering with extragalactic background light, and the result was the same.

rates Γ per dark matter mass M_{DM} . In particular, [43]

$$\frac{\langle\sigma v\rangle J_{\text{cusps}}}{2m_{\chi}^2 M_{\text{DM}}} = \frac{\Gamma}{M_{\text{DM}}} = \frac{1}{m'_{\chi}\tau}. \quad (17)$$

This allows us to deduce straightforwardly the upper limit on $\langle\sigma v\rangle$ given in Fig. 4 for the $\chi\chi \rightarrow b\bar{b}$ annihilation channel from the lower limit on τ derived by a previous study [32] for the $\chi \rightarrow b\bar{b}$ decay channel.

Data availability. No datasets were generated or analysed during this study.

Code availability. Code to evaluate prompt cusp distributions is available from the corresponding author on request. However, it is adapted from code already available at <https://github.com/delos/microhalo-models>.

References

- [1] Roszkowski, L., Sessolo, E. M. & Trojanowski, S. WIMP dark matter candidates and searches—current status and future prospects. *Reports on Progress in Physics* **81** (6), 066201 (2018). <https://doi.org/10.1088/1361-6633/aab913>, <https://arxiv.org/abs/1707.06277> [hep-ph].
- [2] Arcadi, G. *et al.* The waning of the WIMP? A review of models, searches, and constraints. *European Physical Journal C* **78** (3), 203 (2018). <https://doi.org/10.1140/epjc/s10052-018-5662-y>, <https://arxiv.org/abs/1703.07364> [hep-ph].
- [3] H. E. S. S. Collaboration *et al.* Search for dark matter annihilation signals in the H.E.S.S. Inner Galaxy Survey. *arXiv e-prints* arXiv:2207.10471 (2022). <https://arxiv.org/abs/2207.10471> [astro-ph.HE].
- [4] Ackermann, M. *et al.* Searching for Dark Matter Annihilation from Milky Way Dwarf Spheroidal Galaxies with Six Years of Fermi Large Area Telescope Data. *Phys. Rev. Lett.* **115** (23), 231301 (2015). <https://doi.org/10.1103/PhysRevLett.115.231301>, <https://arxiv.org/abs/1503.02641> [astro-ph.HE].
- [5] Hooper, D. & Goodenough, L. Dark matter annihilation in the Galactic Center as seen by the Fermi Gamma Ray Space Telescope. *Physics Letters B* **697** (5), 412–428 (2011). <https://doi.org/10.1016/j.physletb.2011.02.029>, <https://arxiv.org/abs/1010.2752> [hep-ph].
- [6] Grand, R. J. J. & White, S. D. M. Dark matter annihilation and the Galactic Centre Excess. *MNRAS* **511** (1), L55–L59 (2022). <https://doi.org/10.1093/mnrasl/slac011>, <https://arxiv.org/abs/2201.03567> [astro-ph.CO].

- [7] Green, A. M., Hofmann, S. & Schwarz, D. J. The power spectrum of SUSY-CDM on subgalactic scales. *MNRAS* **353** (3), L23–L27 (2004). <https://doi.org/10.1111/j.1365-2966.2004.08232.x>, <https://arxiv.org/abs/astro-ph/0309621> [astro-ph].
- [8] Zavala, J. & Frenk, C. S. Dark Matter Haloes and Subhaloes. *Galaxies* **7** (4), 81 (2019). <https://doi.org/10.3390/galaxies7040081>, <https://arxiv.org/abs/1907.11775> [astro-ph.CO].
- [9] Wang, J. *et al.* Universal structure of dark matter haloes over a mass range of 20 orders of magnitude. *Nature* **585** (7823), 39–42 (2020). <https://doi.org/10.1038/s41586-020-2642-9>, <https://arxiv.org/abs/1911.09720> [astro-ph.CO].
- [10] Ando, S., Ishiyama, T. & Hiroshima, N. Halo Substructure Boosts to the Signatures of Dark Matter Annihilation. *Galaxies* **7** (3), 68 (2019). <https://doi.org/10.3390/galaxies7030068>, <https://arxiv.org/abs/1903.11427> [astro-ph.CO].
- [11] White, S. D. M. Prompt cusp formation from the gravitational collapse of peaks in the initial cosmological density field. *arXiv e-prints* arXiv:2207.13565 (2022). <https://arxiv.org/abs/2207.13565> [astro-ph.CO].
- [12] Ludlow, A. D. *et al.* The mass profile and accretion history of cold dark matter haloes. *MNRAS* **432** (2), 1103–1113 (2013). <https://doi.org/10.1093/mnras/stt526>, <https://arxiv.org/abs/1302.0288> [astro-ph.CO].
- [13] Navarro, J. F., Frenk, C. S. & White, S. D. M. The Structure of Cold Dark Matter Halos. *ApJ* **462**, 563 (1996). <https://doi.org/10.1086/177173>, <https://arxiv.org/abs/astro-ph/9508025> [astro-ph].
- [14] Navarro, J. F., Frenk, C. S. & White, S. D. M. A Universal Density Profile from Hierarchical Clustering. *ApJ* **490** (2), 493–508 (1997). <https://doi.org/10.1086/304888>, <https://arxiv.org/abs/astro-ph/9611107> [astro-ph].
- [15] Navarro, J. F. *et al.* The inner structure of Λ CDM haloes - III. Universality and asymptotic slopes. *MNRAS* **349** (3), 1039–1051 (2004). <https://doi.org/10.1111/j.1365-2966.2004.07586.x>, <https://arxiv.org/abs/astro-ph/0311231> [astro-ph].
- [16] Navarro, J. F. *et al.* The diversity and similarity of simulated cold dark matter haloes. *MNRAS* **402** (1), 21–34 (2010). <https://doi.org/10.1111/j.1365-2966.2009.15878.x>, <https://arxiv.org/abs/0810.1522> [astro-ph].
- [17] Angulo, R. E., Hahn, O., Ludlow, A. D. & Bonoli, S. Earth-mass haloes and the emergence of NFW density profiles. *MNRAS* **471** (4), 4687–4701

- (2017). <https://doi.org/10.1093/mnras/stx1658>, <https://arxiv.org/abs/1604.03131> [astro-ph.CO].
- [18] Delos, M. S., Erickcek, A. L., Bailey, A. P. & Alvarez, M. A. Are ultra-compact minihalos really ultracompact? *Phys. Rev. D* **97** (4), 041303 (2018). <https://doi.org/10.1103/PhysRevD.97.041303>, <https://arxiv.org/abs/1712.05421> [astro-ph.CO].
- [19] Delos, M. S., Erickcek, A. L., Bailey, A. P. & Alvarez, M. A. Density profiles of ultracompact minihalos: Implications for constraining the primordial power spectrum. *Phys. Rev. D* **98** (6), 063527 (2018). <https://doi.org/10.1103/PhysRevD.98.063527>, <https://arxiv.org/abs/1806.07389> [astro-ph.CO].
- [20] Delos, M. S., Bruff, M. & Erickcek, A. L. Predicting the density profiles of the first halos. *Phys. Rev. D* **100** (2), 023523 (2019). <https://doi.org/10.1103/PhysRevD.100.023523>, <https://arxiv.org/abs/1905.05766> [astro-ph.CO].
- [21] Colombi, S. Phase-space structure of protohalos: Vlasov versus particle-mesh. *A&A* **647**, A66 (2021). <https://doi.org/10.1051/0004-6361/202039719>, <https://arxiv.org/abs/2012.04409> [astro-ph.CO].
- [22] Delos, M. S. & White, S. D. M. Inner cusps of the first dark matter haloes: Formation and survival in a cosmological context. *arXiv e-prints* arXiv:2207.05082 (2022). <https://arxiv.org/abs/2207.05082> [astro-ph.CO].
- [23] Amorisco, N. C. Cold dark matter subhaloes at arbitrarily low masses. *arXiv e-prints* arXiv:2111.01148 (2021). <https://arxiv.org/abs/2111.01148> [astro-ph.CO].
- [24] Benson, A. J. & Du, X. Tidal Tracks and Artificial Disruption of Cold Dark Matter Halos. *arXiv e-prints* arXiv:2206.01842 (2022). <https://arxiv.org/abs/2206.01842> [astro-ph.GA].
- [25] Stücker, J., Ogiya, G., Angulo, R. E., Aguirre-Santaella, A. & Sánchez-Conde, M. A. Tidal Stripping in the Adiabatic Limit. *arXiv e-prints* arXiv:2207.00604 (2022). <https://arxiv.org/abs/2207.00604> [astro-ph.CO].
- [26] Drakos, N. E., Taylor, J. E. & Benson, A. J. A universal model for the evolution of tidally stripped systems. *arXiv e-prints* arXiv:2207.14803 (2022). <https://arxiv.org/abs/2207.14803> [astro-ph.GA].
- [27] Peñarrubia, J. *et al.* The impact of dark matter cusps and cores on the

- satellite galaxy population around spiral galaxies. *MNRAS* **406** (2), 1290–1305 (2010). <https://doi.org/10.1111/j.1365-2966.2010.16762.x>, <https://arxiv.org/abs/1002.3376> [astro-ph.GA].
- [28] Bardeen, J. M., Bond, J. R., Kaiser, N. & Szalay, A. S. The Statistics of Peaks of Gaussian Random Fields. *ApJ* **304**, 15 (1986). <https://doi.org/10.1086/164143>.
- [29] Cautun, M. *et al.* The milky way total mass profile as inferred from Gaia DR2. *MNRAS* **494** (3), 4291–4313 (2020). <https://doi.org/10.1093/mnras/staa1017>, <https://arxiv.org/abs/1911.04557> [astro-ph.GA].
- [30] Di Mauro, M. Characteristics of the Galactic Center excess measured with 11 years of Fermi-LAT data. *Phys. Rev. D* **103** (6), 063029 (2021). <https://doi.org/10.1103/PhysRevD.103.063029>, <https://arxiv.org/abs/2101.04694> [astro-ph.HE].
- [31] Ackermann, M. *et al.* The Spectrum of Isotropic Diffuse Gamma-Ray Emission between 100 MeV and 820 GeV. *ApJ* **799** (1), 86 (2015). <https://doi.org/10.1088/0004-637X/799/1/86>, <https://arxiv.org/abs/1410.3696> [astro-ph.HE].
- [32] Blanco, C. & Hooper, D. Constraints on decaying dark matter from the isotropic gamma-ray background. *J. Cosmology Astropart. Phys.* **2019** (3), 019 (2019). <https://doi.org/10.1088/1475-7516/2019/03/019>, <https://arxiv.org/abs/1811.05988> [astro-ph.HE].
- [33] Steigman, G., Dasgupta, B. & Beacom, J. F. Precise relic WIMP abundance and its impact on searches for dark matter annihilation. *Phys. Rev. D* **86** (2), 023506 (2012). <https://doi.org/10.1103/PhysRevD.86.023506>, <https://arxiv.org/abs/1204.3622> [hep-ph].
- [34] Allahverdi, R. *et al.* The First Three Seconds: a Review of Possible Expansion Histories of the Early Universe. *The Open Journal of Astrophysics* **4** (1), 1 (2021). <https://doi.org/10.21105/astro.2006.16182>, <https://arxiv.org/abs/2006.16182> [astro-ph.CO].
- [35] Planck Collaboration *et al.* Planck 2018 results. VI. Cosmological parameters. *A&A* **641**, A6 (2020). <https://doi.org/10.1051/0004-6361/201833910>, <https://arxiv.org/abs/1807.06209> [astro-ph.CO].
- [36] Blas, D., Lesgourgues, J. & Tram, T. The Cosmic Linear Anisotropy Solving System (CLASS). Part II: Approximation schemes. *J. Cosmology Astropart. Phys.* **2011** (7), 034 (2011). <https://doi.org/10.1088/1475-7516/2011/07/034>, <https://arxiv.org/abs/1104.2933> [astro-ph.CO].

- [37] Hu, W. & Sugiyama, N. Small-Scale Cosmological Perturbations: an Analytic Approach. *ApJ* **471**, 542 (1996). <https://doi.org/10.1086/177989>, <https://arxiv.org/abs/astro-ph/9510117> [astro-ph].
- [38] Bertschinger, E. Effects of cold dark matter decoupling and pair annihilation on cosmological perturbations. *Phys. Rev. D* **74** (6), 063509 (2006). <https://doi.org/10.1103/PhysRevD.74.063509>, <https://arxiv.org/abs/astro-ph/0607319> [astro-ph].
- [39] Sheth, R. K., Mo, H. J. & Tormen, G. Ellipsoidal collapse and an improved model for the number and spatial distribution of dark matter haloes. *MNRAS* **323** (1), 1–12 (2001). <https://doi.org/10.1046/j.1365-8711.2001.04006.x>, <https://arxiv.org/abs/astro-ph/9907024> [astro-ph].
- [40] Delos, M. S. Tidal evolution of dark matter annihilation rates in subhalos. *Phys. Rev. D* **100** (6), 063505 (2019). <https://doi.org/10.1103/PhysRevD.100.063505>, <https://arxiv.org/abs/1906.10690> [astro-ph.CO].
- [41] Aguirre-Santaella, A., Sánchez-Conde, M. A., Ogiya, G., Stücker, J. & Angulo, R. E. Shedding light on low-mass subhalo survival and annihilation luminosity with numerical simulations. *arXiv e-prints* arXiv:2207.08652 (2022). <https://arxiv.org/abs/2207.08652> [astro-ph.GA].
- [42] Blanco, C. γ -cascade: a simple program to compute cosmological gamma-ray propagation. *J. Cosmology Astropart. Phys.* **2019** (1), 013 (2019). <https://doi.org/10.1088/1475-7516/2019/01/013>, <https://arxiv.org/abs/1804.00005> [astro-ph.HE].
- [43] Blanco, C., Delos, M. S., Erickcek, A. L. & Hooper, D. Annihilation signatures of hidden sector dark matter within early-forming microhalos. *Phys. Rev. D* **100** (10), 103010 (2019). <https://doi.org/10.1103/PhysRevD.100.103010>, <https://arxiv.org/abs/1906.00010> [astro-ph.CO].

Author contributions. M.S.D. contributed to the design of the project, performed computations and analysis, and wrote the first draft of the paper. S.D.M.W. initially conceived the project, and contributed to its design, analysis of results, and writing of final draft.

Competing Interests. The authors declare that they have no competing interests.

Additional information. Correspondence and requests for materials should be addressed to M.S.D.